Field Oriented Control of Induction Machines Employing Rotor End Ring Current Detection

Takayoshi Matsuo, *Member, IEEE,* Vladimir Blasko, *Member, IEEE,*
Julio C. Moreira, *Member, IEEE,* and Thomas A. Lipo, *Fellow, IEEE*

***Abstract*—The usual method of induction motor torque control uses the indirect field orientation principle in which the rotor speed is sensed and slip frequency is added to form the stator impressed frequency. Unfortunately, the rotor resistance varies as the motor heats up under load thereby changing the rotor time constant which has a deleterious effect on the torque response. In this paper two new field oriented control schemes are presented which employ rotor end ring current detection and thereby remove the dependence of the controller accuracy on temperature so that the controller is entirely independent of rotor time constant variations. The field orientation schemes do not require an incremental encoder for rotor position sensing. The motor torque can be accurately controlled even down to zero speed operation.**

I. Introduction

THE principle of field oriented control is now well established as the standard upon which all induction motor torque controllers are compared, if not, in fact, based. The preferred method of control uses the so-called indirect field orientation principle in which the rotor speed is accurately sensed and slip frequency is added to form the stator impressed frequency [1]. The slip frequency is calculated from a nonlinear function which is dependent upon the rotor time constant. Unfortunately, the rotor resistance varies over a wide range as the motor heats up under load and during low speed operation, thereby changing the rotor time constant and having a deleterious effect on the torque transient response. Also, the rotor inductance is a function of the flux level in the machine varying widely during field weakening operation and, hence causing additional difficulties in regulating torque at high speeds.

Another method of control, termed direct field orientation, is possible [2]. In this scheme, torque is controlled by measuring stator current and air gap flux and, from these measurements, estimating the amplitude and position of the rotor flux. Torque is controlled by direct regulation of the stator current amplitude and phase relative to the rotor flux. This approach is rarely used since the controller is unable to operate reliably to zero speed because of the inaccuracies involved in the flux measurement below several Hertz.

Recently, another method of direct field orientation has been proposed by Magureanu [3], [4] and Yamamura [5]. In this approach, the end ring current is measured by means of Hall effect sensors and the rotor bar current is calculated. The torque is then controlled by adjusting the stator current having the correct phase and amplitude relationship with respect to the rotor current. In these implementations, however, the rotor current must be accurately measured in both amplitude and phase. Unfortunately, the Hall sensors are sensitive to temperature variations so that an accurate measurement of rotor current is difficult.

Manuscript received February 28, 1991; revised May 7, 1994.
The authors are with the Department of Electrical and Computer Engineering, University of Wisconsin-Madison, Madison, WI 53706 USA.
IEEE Log Number 9404428.

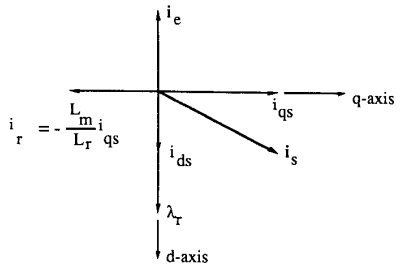

Fig. 1. *d- q* representation of spatial position of machine variables in the steady state.

In this paper two new approaches to induction motor field oriented control are proposed which remove the dependence of the controller accuracy on temperature. The system is therefore considerably more robust than previously reported controllers. The motor torque can be accurately controlled even down to zero speed operation. Moreover, the controller is completely independent of rotor time constant variations.

II. Principle of Field Orientation

A *d-q* axis diagram illustrating the principle of field orientation is shown in Fig. 1. In general, the instantaneous position of the maximum rotor flux density must be located within the machine. In a *d-q* axis representation of the machine, the rotor flux linkage vector forms the circuit equivalent of the rotor flux density and the position of the rotor flux linkage vector must be located upon the *d-q* plane. This spatial position is usually taken to be the *d*-axis as shown in Fig. 1. The excitation of the machine is controlled by the component of stator MMF that is colinear with the peak rotor flux density. The torque of the machine is controlled by maintaining the excitation component of stator MMF constant while producing a varying and proportional amount of stator MMF spatially at right angles to the peak rotor flux density (in electrical degrees). In *d-q* axis diagram it means the proper adjustment of the in-phase (*d*-axis excitation component) and the out-of-phase (*q*-axis torque component) spatial components of stator current relative to the rotor current vector as shown in Fig. 1.

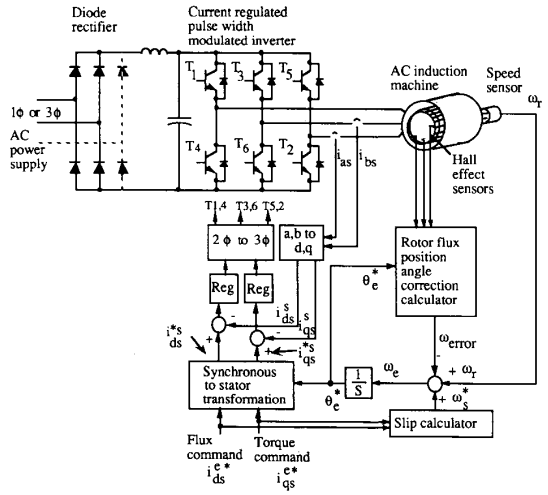

Fig. 2. Indirect field oriented controller using end ring current position sensing.

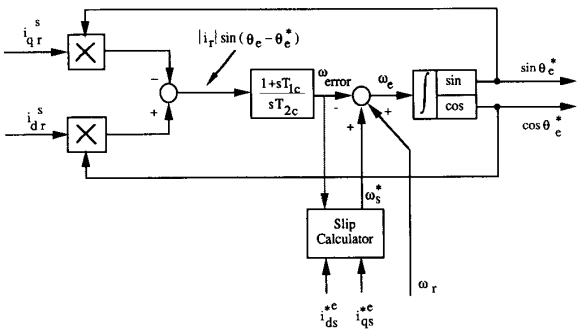

Fig. 3. Method for generating sine and cosine of the rotor flux position utilizing phase locked loop.

It is interesting and important to note from Fig. 1 that the rotor flux linkage vector is always precisely 90 electrical degrees out of phase with the rotor current vector when field orientation is maintained. This result is inherently due to the fact that the voltage across the rotor resistance is equal to the time rate of change of rotor flux linkages. In addition, it is well known that the rotor end ring current produces an MMF distribution that is spatially at right angles with the rotor bar current when expressed in electrical degrees [8]. Hence, the current vector representing the rotor end ring current becomes colinear with the rotor flux linkage vector as illustrated in Fig. 1. The rotor current vector can be obtained from the rotor end ring current vector with a proper transformation of variables and then the rotor flux linkage vector can be formed by adding the stator current vector and the transformed rotor current vector with a proper amplitude ratio.

III. Indirect Field Oriented Controller Utilizing End Ring Current Position Sensing

While measurement of the rotor current is generally impractical with a squirrel cage machine, the rotor end ring leakage flux can, however, be easily measured by placing Hall sensors in the vicinity of the rotor end ring. Since the path of the end ring leakage flux is essentially through air, such a flux measurement is effectively proportional to the rotor end ring current and, with the proper correction factor, to the rotor bar current itself. This signal can now be used as a feedback signal to produce field oriented control. In previous papers, the sensing signal was used as a feedback signal to directly control the rotor currents of the machine [3]–[5]. Unfortunately, Hall sensors are very susceptible to drift so that an accurate measurement of rotor current over a wide operating condition is difficult. Hence, previous direct controllers utilizing rotor current measurement suffer deterioration in performance due to temperature changes in much the same manner as the indirect field oriented controller.

This problem can be overcome by using the sensed signal to determine only the position of the rotor end ring current and, consequently, the position of the rotor flux density (rotor flux linkage). Hence, controller becomes unaffected by the changes of the characteristics of Hall sensors with temperature. A practical control scheme utilizing this concept is shown in Fig. 2. In this example, Hall sensors located near the rotor end ring sense the rotor leakage flux and therefore the bar currents at these points. The correction signal for the rotor flux position angle is calculated by utilizing the sensed rotor current signals. The sine and cosine of the rotor flux position are formed as shown in Fig. 3. These two sinusoidal variations can be used to transform the stator current for torque command and flux command expressed in the synchronous reference frame to equivalent command currents in the stationary reference frame. The resulting command currents are summed with the actual measured currents in d-q form and regulated with a pulse width modulated inverter in the usual manner to form a stator current source of the desired amplitude and phase with respect to the rotor flux linkage.

The scheme for obtaining sine and cosine of rotor flux position, which is shown in Fig. 3, has good filtering capabilities of high frequency components with constant and stable amplitude of output signals. Hall sensor signals are multiplied by sine and cosine of command rotor flux angle. A signal is thus obtained which, when fed through PI controller, zeros any error between the commanded and real rotor flux position. By feeding forward computed rotor flux position angle, the dynamics of the PLL scheme in Fig. 3 can be improved. As in indirect feed forward field oriented control this angle can be calculated on the base of calculated slip frequency and rotor speed. Therefore the output signal from the PI controller in Fig. 3 can be considered as a correction signal which for a properly adjusted slip calculator tends to zero. In addition, the correction signal can be used for slip calculator gain adjustment. Thus, changes of slip controller gain due to temperature variations are compensated.

Although the PLL scheme in Fig. 3 has good filtering properties, additional measures can be used to eliminate the presence of nonfundamental components in the sine and cosine signals. Probably the most severe is the third harmonic and its multiples which arise due to saturation of the machine. This problem can, however, be eliminated by utilizing three Hall

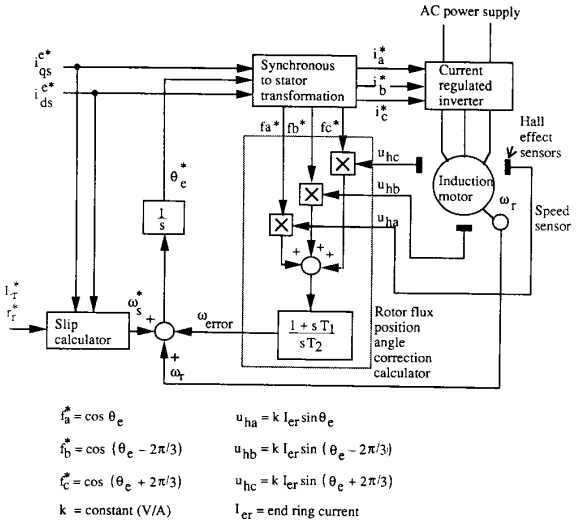

Fig. 4. Compensation schematic eliminating the effect of third harmonic due to saturation.

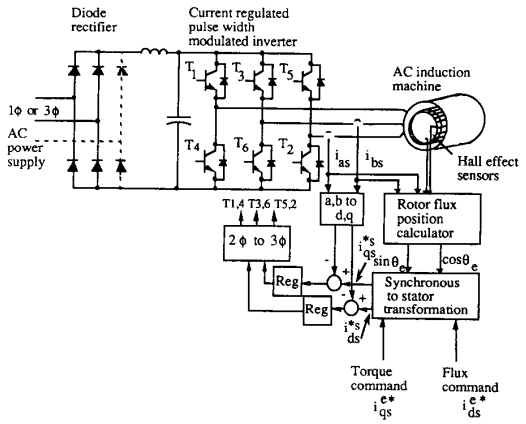

Fig. 5. Direct field oriented controller employing end ring current detection.

sensors in a three phase arrangement as shown in Fig. 4. In this case, third harmonic and other triple components are nulled out when the three product terms are summed.

IV. Direct Field Oriented Controller Employing Rotor End Ring Current Detection

The direct field oriented control scheme, which is proposed here, is shown in Fig. 5. In this example, two Hall sensors, located near to the rotor end ring and spaced by 90 electrical degrees, sense the rotor end ring leakage flux and therefore the bar currents at these two points. Rotor flux is related to the stator and rotor currents by

$$\lambda_{qr}^s = L_m i_{qs}^s + L_r i_{qr}^s \quad (1)$$

$$\lambda_{dr}^s = L_m i_{ds}^s + L_r i_{dr}^s \quad (2)$$

Normalizing these signals by their amplitude, the sine and cosine of the rotor flux position can now be formed. That is,

$$\sin\theta_e = \lambda_{qr}^s / \lambda_{dqr}^s \quad (3)$$

$$\cos\theta_e = \lambda_{dr}^s / \lambda_{dqr}^s \quad (4)$$

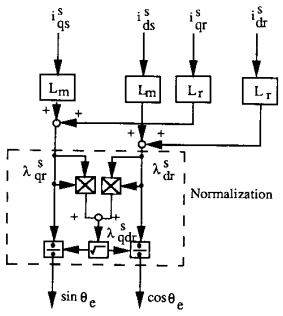

Fig. 6. Rotor flux position calculator.

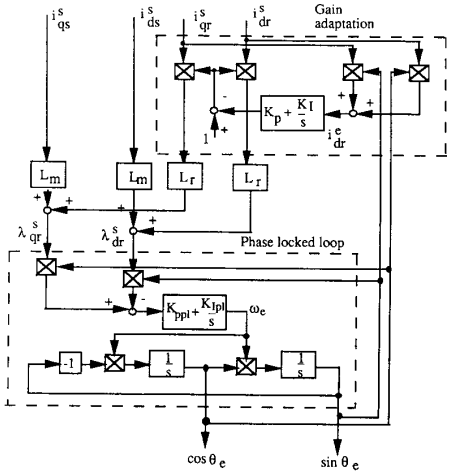

Fig. 7. Rotor flux position calculator with adaptive rotor current referral ratio employing phase locked loop.

where

$$\lambda_{dqr}^s = \sqrt{\lambda_{qr}^{s2} + \lambda_{dr}^{s2}} \quad (5)$$

The basic flux position calculator obtained from these equations is shown in Fig. 6. The two sinusoidal variations, (3) and (4), can be used to transform the stator current for torque command, $i_{qs}^{e^*}$, and flux command, $i_{ds}^{s^*}$, expressed in the synchronously rotating reference frame, to equivalent command currents, $i_{qs}^{s^*}$ and $i_{ds}^{s^*}$, in the stationary reference frame. The resulting command currents, $i_{qs}^{s^*}$ and $i_{ds}^{s^*}$, are summed with the actual measured currents in d, q form and regulated by means of a pulse width modulated inverter. Hence, stator currents of desired amplitude and phase with respect to the rotor flux linkage are produced.

The terms related to rotor current in (1) and (2) are, however, affected by changes of temperature of the Hall sensors. To overcome this problem a rotor flux position calculator utilizing adaptive gain of the rotor current can be introduced as shown in Fig. 7. Adaptation is based on an index of performance which requires the d-axis component of rotor current in synchronous reference frame to be maintained at the value of zero. The d-axis component of rotor current in synchronous reference frame can then be written as

$$i_{dr}^e = i_{qr}^s \sin\theta_e + i_{dr}^s \cos\theta_e \quad (6)$$

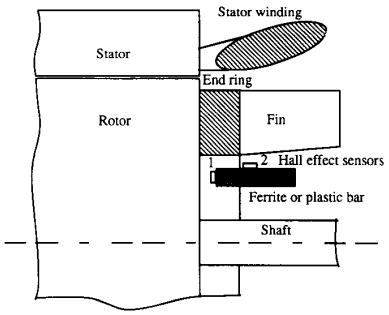

Fig. 8. Cross sectional view of the induction machine showing location of one of the sets of Hall effect sensors.

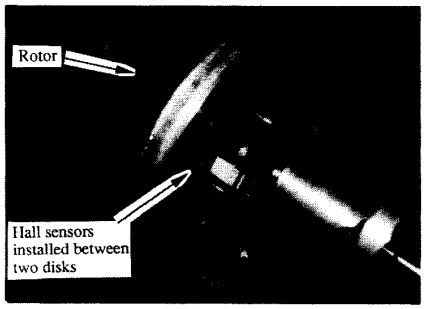

Fig. 9. Rotor and Hall effect sensor arrangement before installation in the induction machine.

which tends to zero, provided that the commanded and real rotor flux vectors are equal. The adaptive loop in Fig. 7 can be viewed as an additional servo drive that keeps the brushes of an equivalent dc machine in the neutral zone resulting in no interaction between the armature and the field circuit. The phase locked loop, which is shown in Fig. 7, can be used to form the sine and cosine of rotor flux position without losing control response or stability and is effective for rejecting harmonic components of the rotor flux signal. Note that in the proposed scheme the rotor flux position is directly sensed. No incremental encoder or other device for sensing rotor position is necessary.

V. End Ring Current Detection

Fig. 8 illustrates a cross-sectional view of the stator and rotor end parts, showing the arrangement of the two Hall effect sensors which were fixed to either a ferrite or a plastic bar. Three of these sets were mounted around the end ring bar and displaced by 120 electrical degrees with respect to each other. These sensors were installed in a 7.5 HP, 4 pole, 230 V induction machine, the rotor of which is shown in Fig. 9, together with the two disks used to install the Hall sensors. Note that this arrangement of the Hall sensors does not require any extensive mechanical adaptation or change in the rotor geometry since the sensors do not physically rotate nor do they come in contact with the rotor.

Experimental results have demonstrated that the signals from Hall sensors 1 and 2 in Fig. 8 are, respectively, 75% and

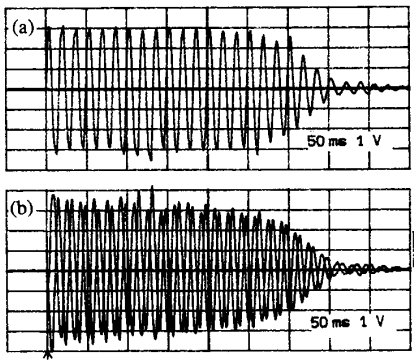

Fig. 10. Experimental results of three phase Hall sensor signals (rotor end ring currents) during starting transient of induction machine at 50% of rated voltage. (a) Phase A Hall sensor signal, 1 volt/div. (b) Phase B and phase C Hall sensor signals, 1 volt/div. Time scale is 0.05 s/div.

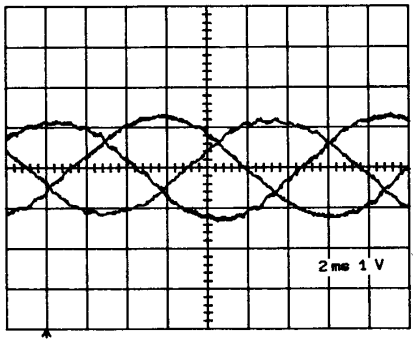

Fig. 11. Three phase hall sensor signals (end rign currents) during rated load condition operating at rated speed, 1 volt/div. Time scale is 2 ms/div.

62% larger than the signals obtained when no ferrite is used. The ratio between signals from sensors 1 and 2 (v_{s1}/v_{s2}), is 0.75 when the machine is operating under rated conditions. The ratio between the signal produced by the end ring current and the signal produce by the stator current is 4.0 for sensor 1, and 1.8 for sensor 2 at the rated conditions. Although the signal from sensor 2 is somewhat larger, the signal from sensor 1 was found to be less influenced by the stator end winding flux leakage and thus the position occupied by the sensor 1 was determined to provide better results. Hence, the position of sensor 1 using a plastic bar is suggested for future research work. A photo of the physical layout showing the installed Hall sensors is shown in Fig. 9.

The signals from the three Hall sensors of position 1, represented the instantaneous value of the end ring current, are plotted in Fig. 10 for a motor starting transient at 50% of rated voltage. Note that the traces are at line frequency since the Hall probes do not rotate with the rotor. Hence, it can be said that the Hall probes essentially accomplish a transformation of variables from a rotating to a stationary reference frame. It is interesting to note that this trace is virtually identical in form to the simulation traces for rotor currents obtained in the stationary reference frame for this same machine [6].

Fig. 11 shows an expanded trace of the rotor end ring current measured for the rated load condition. Note that the three phase signals are nearly balanced and are properly phase

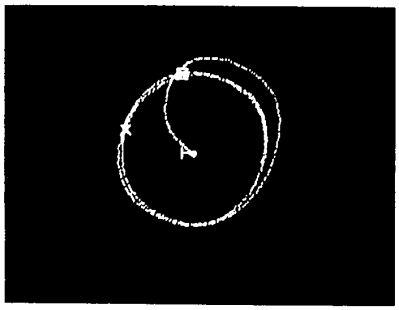

Fig. 12. x- y plot of the two leakage components of end ring flux (end ring current) during initial portion of starting transient.

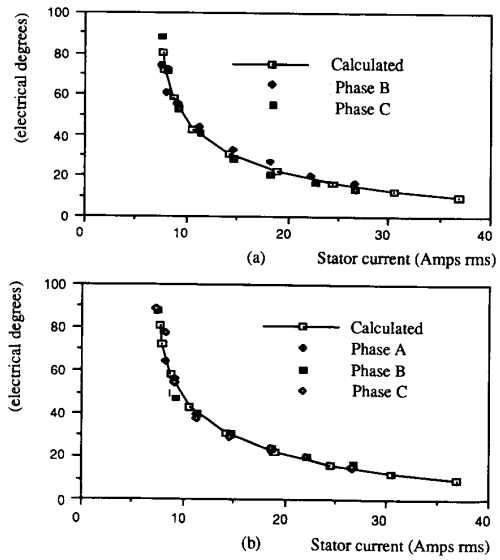

Fig. 13. Calculated and measured angles between stator and rotor currents for arrangement with (a) ferrite core and (b) without the core for the configuration shown in Fig. 8.

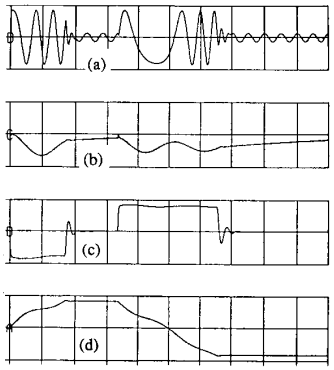

Fig. 14. Starting transient, acceleration, and subsequent loading of 7.5 HP induction motor with indirect field oriented control. Slip calculator assumed to be in error by a factor of 2: (a) stator current, 60 A/div. (b) d-axis rotor current, 10 A/div. (c) q-axis rotor current, 60 A/div., (d) rotor speed, 1200 rpm/div. Time scale is 0.06 s/div.

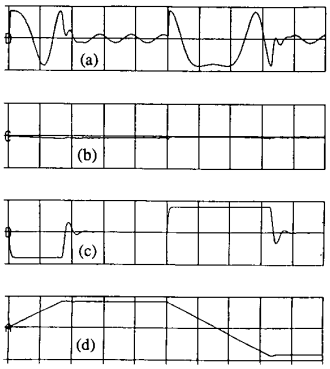

Fig. 15. Starting transient, acceleration, and subsequent loading of 7.5 HP induction motor with indirect field oriented control and feedback correction utilizing Hall sensors. Slip calculator assumed to be in error by a factor of 2: (a) stator current, 60 A/div. (b) d-axis rotor current, 10 A/div. (c) q-axis rotor current, 60 A/div., and (d) rotor speed, 1200 rpm/div. Time scale is 0.06 s/div.

displaced by 120 degrees. Fig. 12 shows an experimental x-y trace of the two components of the Hall probe measurements plotted one versus the other during the initial starting period of the induction machine. Note that the trace rapidly assumes a circular trace indicating a good phase balance between the two components.

The measured and calculated angles between stator and rotor currents are provided in Figs. 13(a) and 13(b) for the arrangement as shown in Fig. 8 with and without the ferrite bar, respectively. Note the good agreement between calculated and measured values obtained in both cases. These results confirm the feasibility of rotor current vector detection in a simple and low cost manner.

VI. Experimental and Computed Results

Typical simulation traces of an indirect field oriented controller are shown in Figs. 14 and 15. Fig. 14 shows the starting transient, acceleration, and subsequent loading of a particular 7.5 HP, 60 Hz, 4 pole induction machine when the slip estimator of the basic indirect field oriented controller of Fig. 2 (without angle corrector) is incorrectly set to twice the correct slip frequency. The power converter used as a part of this simulation is a high frequency ac link resonant converter [7]. Note that the d-axis current is substantially in error resulting in extended acceleration time and overshoot upon reaching the commanded speed. The same starting transient is shown in Fig. 15 with acceleration and subsequent loading when the compensation signal of Fig. 4 is applied. Note that the d-axis rotor current is rapidly zeroed with nearly ideal transient response.

Figs. 16 and 17 show experimental results obtained on actual hardware. In particular, a 7.5 HP, 60 Hz, 4 pole machine simulated in Figs. 14 and 15 was used as the test motor. Again the feed forward controller was incorrectly set to twice the correct slip frequency. In this case, large oscillations are actually noticed at light loads during speed reversal as shown in Fig. 16(a). As shown in the results in Fig. 10(b), these

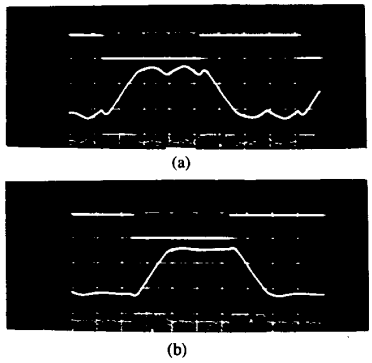

Fig. 16. Waveforms of speed command and actual speed for step reversal in speed command. Rotor time constant assumed to be in error by a factor of 2: (a) with conventional field oriented control, and (b) with field oriented control and the angle correction signal of Fig. 4. Top trace: speed command, 1400 rpm/div., bottom trace speed response, 700 rpm/div. for both figures. Time scale is 0.79 s/div.

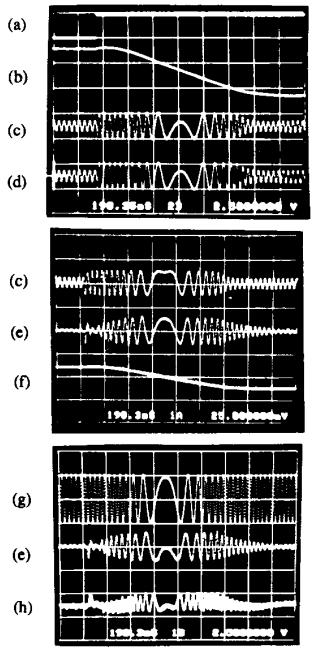

Fig. 17. Waveforms for step reversal in speed command. Same conditions as Fig. 16(b): (a) rotor speed reference, 1400 rpm/div. (b) rotor speed, 700 rpm/div. (c) stator current, 50 A/div. (d) stator current reference, 50 A/div., (e) rotor current, 50 A/div. (f) rotor speed, 1400 rpm/div. (g) cos θ_e, 10 volts/div. (h) output of multiplier multiplying (f) and (g), 25 volts/div. Time scale is 0.2 s/div.

oscillations disappear when the nonlinear feedback controller, as depicted in Fig. 4, is utilized. Traces of some important system variables during reversing of the induction machine speed for a step change with rotor angle position feedback signal in service is presented in Fig. 17. Excellent regulation of all variables is achieved.

Typical simulation traces of the proposed direct field oriented controller are shown in Figs. 18 and 19. Fig. 18 shows

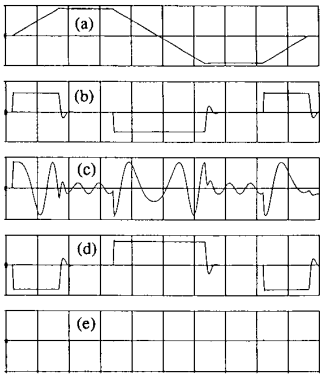

Fig. 18. Acceleration and speed reversal of 7.5 HP induction motor with the direct field oriented control scheme according to Fig. 5: (a) rotor speed, 1200 rpm/div. (b) motor torque, 100 N-m/div. (c) stator current, 60 A/div. (d) q-axis rotor current, 60 A/div. (e) d-axis rotor current, 60 A/div., and time scale is 0.05 s/div.

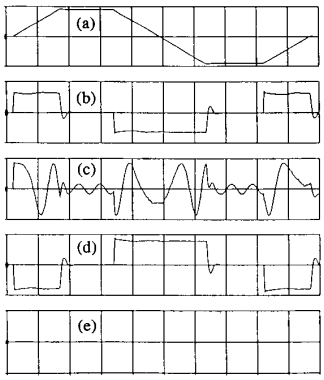

Fig. 19. Acceleration and speed reversal of 7.5 HP induction motor with the direct field oriented control scheme according to Fig. 5. Rotor current signals are assumed to be in error by −6%: (a) rotor speed, 1200 rpm/div. (b) motor torque, 100 N-m/div. (c) stator current, 60 A/div. (d) q-axis rotor current, 60 A/div. (e) d-axis rotor current, 60 A/div., and time scale is 0.05 s/div.

the acceleration and speed reversal from 900 rpm to –900 rpm for a 7.5 HP, 60 Hz, 4 pole induction motor loaded with additional inertia equal to the inertia of rotor. In Fig. 19 the same acceleration and speed reversal is shown for the electrical drive controller of Fig. 5. In this case, however, it was assumed that the rotor current signal was –6% in error because of temperature changes. It should be noted that when driven by the constant current amplifier method the Ga–As Hall sensor used for the experimental portion of the study has an output voltage change of ΔVMAX –0.06%/degree Celsius. Hence, this sensitivity results in an error in the rotor current readings of same value of –6% when the operating air temperature changes +100 degrees Celsius from the temperature at which the gain adjustment was set. Note that the desired torque continues to be developed and that the d-axis component of rotor current is maintained at a negligibly small value.

A digital signal processor based direct field oriented controller has been designed and implemented experimentally

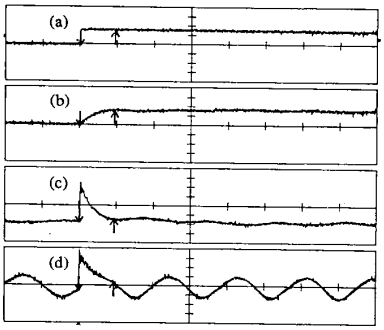

Fig. 20. Experimental waveforms of motor speed, and stator current during speed step change from 250 rpm to 300 rpm: (a) rotor speed reference, 30 rpm/div. (b) rotor speed, 30 rpm/div. (c) stator current i_{qs}^{e} in synchronous reference frame, 5 A/div. (d) stator current i_{as}, 5 A/div., and time scale is 50 ms/div.

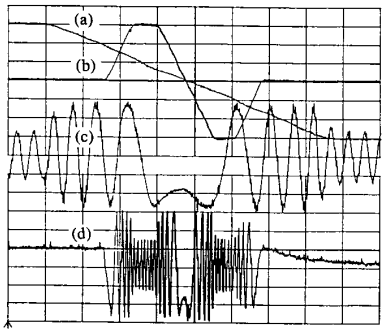

Fig. 21. Experimental waveforms of motor speed and stator current for four quadrant operation: (a), (b) rotor speed, 210 rpm/div. (c), (d) stator current i_{as}, 5 A/div. Time scale for (a) and (c) is 0.1 s/div. and 0.5 s/div. for (b) and (d). Wave forms (a) and (c) are expanded from wave forms (b) and (d), respectively, in terms of horizontal time scale.

in hardware in the laboratory wherein a current regulated pulse width modulated inverter was used to drive a 7.5 HP, 60 Hz, 4 pole induction rotor. The results obtained from this experimental system are shown in Figs. 20 and 21. In particular, Fig. 20 shows transient response of the system resulting from step changes in the speed command. Note that the drive system responds in roughly 25 ms. Fig. 21 shows the behavior of the experimental system during speed reversals. Traces (b) and (d) show the actual rotor speed and stator current during a speed ramp in the positive direction, reversal to the same speed in the reverse direction and then a speed ramp back to zero speed. In traces (a) and (c) the speed reversal portion of the speed profile is shown. Clearly, control of the speed of the machine is excellent even through the region of zero speed.

VII. Conclusion

In this paper two new types of field oriented controllers have been presented. The control concept utilizes the measurement of the rotor end ring current phase position but not the measurement of the current amplitude. The primary advantage over previous controllers is the elimination of the inaccuracies in the Hall probes produced by temperature variations. In this manner the field oriented controller remains robust for air temperature within the machine reaching 150 degrees Celcius.

References

[1] K. Hasse, "Zur Dynamik Drehzahlgeregelter Antriebe Mit Stromrichtergespeisten Asynchron—Kurzschlublaufermaschinen," Ph.D. dissertation, Tech. Hochschule Darmstadt, July 17, 1969.
[2] F. Blaschke, "Das Verfahren der Feldorientierung zur Regelung der Drehfeld-maschine," Ph.D. dissertation, T. U. Braunschweig, 1973.
[3] R. Magureanu, L. Kreindler, D. Floricau, and C. Solacolu, "Current versus voltage control of induction motors operating at constant rotor flux," presented at the IEE Int. Conf. Electrical Machines and Drives, London, 1988.
[4] {-}{-}, "Wide range speed control of induction motors," presented at the Int. Conf. Electric Drives, Poiana Brasov, Roumania, Sept. 20–22, 1988.
[5] S. Yamamura, "Secondary current feedback control of induction motor torque," presented at the Int. Conf. Electric Drives, Poiana Brasov, Roumania, Sept. 20–22, 1988.
[6] J. O. Ojo and T. A. Lipo, "An improved model of saturated induction machines," in *Conf. Rec. 1988 IEEE Ind. Appl. Soc. Annu. Meeting*, pp. 222–230.
[7] S. K. Sul and T. A. Lipo, "Design and performance of a high frequency link induction motor drive operating at unity power factor," in *Conf. Rec. 1988 IEEE Ind. Appl. Soc. Annu. Meeting*, pp. 308–313.
[8] M. Liwschitz-Garik and C. C. Whipple, *Electric Machinery, Volume II, A-C Machines*. New York: Van Nostrand, 1946.

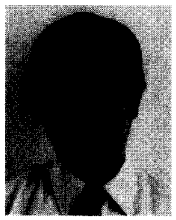

Takayoshi Matsuo (S'90–M'94) was born in Himeji, Japan. He received the B.E. degree in electrical engineering and the M.E. degree in applied electronics from Tokyo Institute of Technology, Japan, in 1975 and 1977, respectively, and the M.S. and Ph.D. degrees in electrical engineering from the University of Wisconsin-Madison in 1983 and 1994, respectively.

From 1977 to 1989 he was an Electrical Engineer in the Power Electronics Department of the Mitsubishi Electric Corporation, Japan. From 1989 to 1994, he was a research assistant while pursuing the Ph.D. degree in the Department of Electrical and Computer Engineering of the University of Wisconsin-Madison. Since 1994, he has been a Research Associate at the University of Wisconsin-Madison. His research interests are in ac drives, power electronics, and electrical machines.

Vladimir Blasko (M'89) received the B.Sc., M.Sc., and Ph.D. degrees in electrotechnical engineering from Electrotechnical Faculty of Zagreb, Croatia, in 1976, 1982, and 1986, respectively.

From 1976 to 1988 he worked at the Electrotechnical Institute Rade Koncar, Zagreb, Croatia, in the Department of Power Electronics and Automatic Control. During the academic year 1988–1989 he was with the University of Wisconsin—Madison as a recipient of the IREX scholarship. From 1989 to 1992 he was with the Research and Development Center of the Otis Elevator Company, Farmington, CT. Since 1992 he has been with Standard Drives Business Division of Allen–Bradley Company. He has been working on the research, development, and design of high power transistor choppers, drives for electrical vehicles, high performance ac elevator drives, and low harmonics regenerative three phase voltage source converters. His primary areas of interest are ac drives, intelligent power management, power electronics, modern control technology, and algorithms.

Julio C. Moreira (S'88–M'90) was born in São Paulo, Brazil, where he received the B.S. and M.S. degrees in electrical engineering from the State University of Campinas in 1979 and 1983, respectively, and the Ph.D. degree in electrical engineering from the University of Wisconsin-Madison in 1990.

He worked as an Engineer and later as a Vice-Coordinator of the Electric Drive Systems Research Laboratory at the State University of Campinas in Brazil from 1980 to 1985. In 1981 he became a Researcher and an Assistant Professor at that same institution, teaching courses in electrical machines, power electronics, industrial electronics, servo drive controls, and microprocessors. His research activities included the development of dc and ac motor drives systems for public transportation and for electric vehicles. He also served as a consultant in the areas of electric drive systems and switched mode power supplies. After receiving the Ph.D. he joined the Whirlpool Corporate Research and Engineering Center, MI, as a Lead Engineer, where he is involved with research in the areas of power electronics, electric machines design, electric motor drive systems, and digital controls.

Dr. Moreira is a member of the IEEE Power Electronics Society, the IEEE Industry Applications Society, and the IEEE Industrial Electronics Society. He has received two IEEE prize paper awards and has two patents pending.

Thomas A. Lipo (M'64–SM'71–F'87) is a native of Milwaukee, WI. He received the B.E.E. and M.S.E.E. degrees from Marquette University, Milwaukee, in 1962 and 1964, respectively, and the Ph.D. degree in electrical engineering from the University of Wisconsin in 1968.

From 1969 to 1979 he was an Electrical Engineer in the Power Electronics Laboratory of Corporate Research and Development of the General Electric Company, Schenectady, NY. He became Professor of Electrical Engineering at Purdue University in 1979 and in 1981 he joined the University of Wisconsin in the same capacity,where he is presently the W. W. Grainger Professor for Power Electronics and Electrical Machines.

Dr. Lipo has been engaged in power electronics research for over 25 years. He has received 17 IEEE prize paper awards for his work, including co-recipient of the Best Paper Award in the IEEE Industry Applications Society TRANSACTIONS for the year 1984. In 1986 he received the Outstanding Achievement Award from the IEEE Industry Applications Society for his contributions to the field of ac drives and in 1990 he received the William E. Newell Award of the IEEE Power Electronics Society for contributions to the field of power electronics. He currently serves as the President of the IEEE Industry Applications Society.